A Numerical Study of Air-Bearing Slider Form-Factors

Brian H. Thornton and David B. Bogy

Computer Mechanics Laboratory
5129 Etcheverry Hall
Department of Mechanical Engineering
University of California
Berkeley, CA. 94720

ABSTRACT – This paper presents a numerical study comparing the performance of air bearing slider form-factors. The air bearing slider and air bearing surface (ABS) design has gone through drastic changes in recent years in order to achieve the performance required by lower flying heights. In the past, improvements have been seen by scaling down the form-factors of air bearing sliders. The pico form-factor (1.25 × 1 mm) has been successfully used for several generations of products and the question arises – should the form-factor be scaled down further? The dynamic characteristics and flying-height modulation (FHM) performance of two different ABS designs in the pico and femto (0.82 × 0.66 mm) form-factors were numerically investigated. It was found that for the smaller form-factor designs, greater damping of the air bearing film and slider body system was achieved but with an undesirable decrease in modal frequencies. However, depending on the ABS design, beneficial dynamic properties can be achieved by scaling down the form-factor from pico to femto. Maximizing the total air bearing force (the sum of negative and positive) with a design featuring a large number of transverse pressure gradients can obtain high stiffness and damping. Geometric FHM was also investigated using both sinusoidal disk waviness and an actual measured disk topography. It was found that the FHM depends not only on the form-factor, but also on the ABS design. For long disk waviness wavelengths (longer than the slider body length, L), the FHM is proportional to L^b where b was found to be between 2.6 and 4; hence FHM is dependent on form-factor. For short disk waviness wavelengths, the FHM is a function of the ABS design and flying attitude and not form-factor. A disk waviness wavelength of 3 mm demarks the transition above which the FHM is a function of form-factor and below which the FHM is a function of the ABS design and the superposition of these two effects compose the geometric FHM. Simulations with an actual measured disk topography showed that the femto form-factor exhibited 22% - 32% less FHM than the pico form-factor for a similar design. However, by changing the ABS design, 35% - 40 % less FHM was achieved within the same form-factor. By scaling down a pico slider to a femto slider, we do not necessarily achieve enhanced overall performance. Significant performance improvements in the pico form-factor can be attained if the ABS is properly designed. However, in designing a dynamically stable and low FHM air bearing slider a femto slider ultimately yields better performance when care is taken in designing the ABS.

INTRODUCTION

In the evolution of hard disk drives, there has been a steady trend toward miniaturization of the drives as well as all its components. This miniaturization is motivated by several considerations such as economics, higher areal magnetic densities, access time and data rate, physical space requirements, and new applications other than computer data storage. While the general design of the mechanical components of disk drives has remained relatively fixed, the air bearing slider design has gone through substantial changes. The slider housing the read/write transducer has evolved from a large aluminum externally pressurized hydrostatic slider in 1957 with head/media spacing of 20 μm to today's complex self-acting ceramic pico (30%: 1.25 mm × 1 mm) air bearing sliders flying at sub-20 nm over the media [1]. The need for more complex air bearing designs stems from the higher bit areal densities requiring a smaller gap, or flying-height (FH) between the transducer and magnetic media. In turn, this has increased the need for a better understanding of the head-disk interface. Shrinking the air bearing slider form-factor has produced many benefits both economical and in performance. As the FHs approach the sub-5 nm range the natural question arises: is it time to scale the form-factor down once again too keep up with the rapidly increasing performance criteria?

For a recording density of 1 Tbit/in^2, it is projected that the FH will be 3.5 nm [2]. In order for a reliable head-disk interface to be maintained, contact between the slider and disk and fluctuations in FH need to be held to a minimum. Therefore, the dynamic performance of air bearing sliders is becoming of increasing importance. At such low FH's, intermittent contacts between the slider and the disk are unavoidable. The more stable the air bearing slider, the less damage will occur and the faster the slider will settle back to its steady-state flying condition once disturbed. Important characteristic parameters controlling the stability are the air bearing modal frequencies and damping ratios. The higher the frequencies and damping ratios, the more stable the interface. The spacing fluctuations between the transducer and disk, or FHM, also needs to be held to a

minimum. A large fraction of the FHM is the so-called "geometric" FHM [3-5]. This FHM occurs due to disk waviness and micro-waviness with significant amplitude in the wavelength range from approximately 8 mm down to the wavelength corresponding to the first air bearing natural frequency – on the order of several hundred microns [3]. It has been shown for disk waviness wavelengths much longer than the slider body length, *L*, that the geometric FHM scales proportionally to the square of the slider body length [5]. Also, from more recent studies, in the waviness wavelength regime where the wavelength is comparable to the slider body length, this geometric FHM becomes a very complex function of the ABS geometry and attitude and not the slider's length [3].

In order for manufacturers to decrease the slider form-factor, the benefits must outweigh the costs involved. A study is presented here comparing the dynamic and FHM performance as a function of form-factor and ABS design for two sizes of air bearing sliders.

AIR BEARING DESIGNS

In this paper we investigated two ABS designs of different rail complexity. The first design, depicted in Fig. 1a, is a five-pad sub-ambient pressure design labeled ABS I. The second and more complicated design is a sub-ambient pressure design shown in Fig. 1b labeled ABS II. The transducer is located near the center of the trailing edge of the slider body. ABS I was designed with the following considerations: (1) high stiffness, (2) constant roll angle from inner diameter (ID) to outer diameter (OD), and (3) ease of manufacturing. ABS II was designed with the following considerations: (1) low geometric FHM, (2) high damping, and (3) relatively high stiffness. The simulations were preformed at 7200 RPM, disk radial position of 16.25 mm, and skew angle of zero degrees. Each of the two designs were scaled for pico (30%: 1.25 X 1 mm) and femto (20%: 0.82 X 0.66 mm) form-factors. In changing the form-factor, the geometry of the rails, recess heights, crown, and camber of the ABS's were scaled proportionally as seen in Table 1. The additional features on the leading edge of ABS II protrude 40 nm from the ABS. These additional features serve to increase damping (as will be discussed) and could be manufactured similar to diamond-like carbon pads used on padded "stiction-free" sliders. For this study the FH at the transducer was kept approximately the same for

all designs, but due to the highly non-linear nature of the generalized Reynolds equations, the gram-load could not simply be scaled down proportionally, as seen in Table 1. The static attitude of each ABS is also shown in Table 1. ABS I and ABS II were designed for transducer FHs of 7 nm and 5 nm, respectively for 100 Gbit/in^2 and greater areal recording density applications. Figures 2a and 2b show the pressure profiles normalized by the ambient pressure generated under the ABS I and ABS II sliders in the pico form-factor, respectively. For each slider design, the pressure profile geometry remained relatively constant, independent of form-factor with differences only in the amplitudes of pressure. The high pressure generated at the side rails of ABS I help achieve high stiffness (especially in the roll motion) and constant roll angle from ID to OD. The features on the trailing edge pad of ABS II help generate high pressure near the transducer location decreasing the geometric FHM and the large number of pressure gradients generated on the leading edge pads increase the air film damping [3],[6].

DYNAMIC SYSTEM PROPERTIES OF THE AIR BEARING

The air bearing film and slider body form a complex coupled non-linear dynamic system. By using the CML Dynamic Air Bearing Simulator, which solves the generalized Reynolds equations coupled with the dynamics of the slider body and a lumped parameter suspension, we are able to simulate the dynamic response of the slider for various inputs. For small perturbations about the slider's steady flying attitude the non-linearities are small and linear modal analysis can be used to obtain the modal parameters of the air bearing slider system. This system is modeled as a three degree-of-freedom (DOF) system – the vertical, pitch and roll motions. By simulating the response of the slider to initial velocities in all three DOFs, we can estimate the impulse response functions and perform modal analysis to obtain the modal masses, stiffnesses, damping ratios and nodal lines [6]. The modal frequencies and damping ratios are shown in Figs. 3 and 4 for the ABS I and ABS II designs, respectively, for the two form-factors investigated. Modes 1, 2 and 3 correspond to the three coupled modes generally called pitch, roll, and vertical or first-pitch, roll and second-pitch. For the ABS I designs, modes 1, 2 and 3 correspond to the first-pitch, roll, and second-pitch, respectively. For ABS II, modes 1, 2, and 3 correspond to roll, first-pitch and second-pitch, respectively.

The modal parameters are dependent on the pressure profile generated under the ABS and the size and mass of the slider body. The nodal lines or mode shapes remain relatively fixed for each design regardless of form-factor as expected by the relatively constant pressure profiles generated by each design in the two form-factors. However, the modal stiffnesses and damping ratios changed drastically with form-factor, as seen in Figs. 3 and 4, due to several effects.

As the sliders decrease in size, all three modal frequencies of both slider designs decrease. This result my seem counter-intuitive initially due to the smaller mass of the smaller form-factor (i.e. the modal frequency w_i @ $(k_i/m_i)^{0.5}$), however the stiffness decreases significantly more than the mass causing the modal frequencies to ultimately decrease with decreasing form-factor.

There are two effects that cause the stiffness to decrease as slider size decreases. As the form-factor decreases, so does the bearing load capacity – the ability of the air bearing to create positive and negative forces. For a decrease in length dimension by 33 % (pico to femto) the ABS area decreases by 56 %. The forces generated by the air film are related to the area that the air pressure acts over; hence by decreasing the area, so will the bearing load capacity. ABS I decreases its load capacity by 60 % and 58 % to produce positive and negative force, respectively as seen in Table 1. Similarly, ABS II decreases its load capacity by 48 % and 53 % to produce positive and negative force, respectively. The ability of a slider design to retain load capacity while reducing the form-factor helps it to maintain a stiff air bearing film. Scaling the form-factor from pico to femto causes total force (positive force + | negative force |) to decrease by 59% and 51% for ABS I and ABS II, respectively. The ability of ABS II to retain a larger percentage of the total force helps it retain its stiffness as the form-factor is decreased.

Peak pressures generated by the air bearing can also have an effect on air bearing stiffness. The higher a pressure peak, the stiffer the local area will be. ABS I contains three high pressure points – one at the trailing edge pad and two on the side rails demarked in Fig. 2 as locations A and B. These three locations can be viewed as three stiff distributed springs over the local areas of the pads. When the form-factor decreases from pico to femto, the overall effectiveness of these three springs decreases as the peak pressures decrease (see Table 2). However, ABS II has only one high pressure point

located on the trailing edge pad as seen in Fig. 2, and as the form-factor decreases from pico to femto, the peak pressure actually increases. This increase in peak pressure helps to maintain the stiffness of ABS II in the femto form-factor. This is most effective in retaining the stiffness of the pitch modes exhibiting a decrease of only 4.6 % in stiffness for ABS II when it is scaled down from pico to femto as compared to a 30.4 % decrease in stiffness of ABS I. The three high pressure points on ABS I provide the characteristic high stiffness, especially in the roll direction, however, when it is scaled down from pico to femto, the peak pressures at all three points decrease, hence causing a decrease in all three modal frequencies.

Desirable higher damping ratios were obtained with the femto form-factor as compared to the pico form-factor for both ABS designs. It has been shown previously that the stiffer the air bearing film, the smaller the damping will be (achieved through the transverse viscous shearing [6]-[9]). This holds true for ABS I and ABS II – the femto form-factors have lower stiffnesses than the pico, and hence, higher damping ratios. ABS I had an increase in damping ratios of 1 % to 28 % while ABS II had an increase in damping ratios by at least 30% when scaling the form-factors from pico to femto. Textured ABS designs and disks have been studied and have been shown to enhance the damping characteristics of the air film [6],[7],[10]. The extra pads that are located on top of the leading edge surface of ABS II cause multiple pressure gradients designed to increase damping. From the modal analysis results, it is seen that in comparing the pico form-factors, ABS II exhibits an increase of 21 %, 428 %, and 195 % in damping ratios over ABS I for the pitch, roll, and vertical modes, respectively. Similarly, in comparing the femto form-factors, ABS II exhibited 26 %, 480 %, and 346 % increase in damping ratios over ABS I of the pitch, roll, and vertical modes, respectively.

AIR BEARING FLYING-HEIGHT MODULATION

It has been shown previously that geometric FHM due to disk waviness and micro-waviness can be comparable to the FH [3,4]. It also has been known for some time that for waviness wavelengths much longer than the sliders overall body length the FHM scales proportionally to the square of the slider's length [5]. However, when the waviness wavelength approaches the sliders length, it has more recently been shown that

the FHM is a complex function of the ABS design, and it is independent of the overall length of the slider [3,4]. In order to assess how each ABS design and form-factor is affected by disk waviness, we performed simulations using a modeled sinusoidal disk waviness, *d(x)*, for which the wavelengths, λ, ranged from 20 mm to 0.3125 mm:

$$d(x) = A\sin\left(\frac{2p}{l}x\right) \qquad (1)$$

In this wavelength range, the dynamic resonant modes of the air bearings are not excited and the FHM is a result of geometric effects and not dynamics. The results of the simulations are shown in Figs. 5 and 6. These figures show amplitude ratios of the FHM peak-to-peak ($FHM_{p\text{-}p}$) over the disk waviness amplitude peak-to-peak ($DISK_{p\text{-}p}$), or the "gain" as a function of disk waviness wavelength on a log-log scale. These results are similar to those previously found [3]. The predicted behavior is present, with low gain for disk waviness wavelengths much longer than the slider body length, and with the gain exponentially increasing as the wavelength approaches the slider body length. It is also seen, for long wavelengths, that the larger form-factors exhibit larger gain. However, as the wavelength decreases, the gain becomes dependent on the ABS design and independent of form-factor. This can be seen more clearly in Fig. 7 where the data plotted in Figs. 5 and 6 are plotted on the same plot on a linear-linear scale. There appears to be a transition waviness wavelength (depicted in Fig. 7) at approximately 3 mm – above which the FHM is dependent on the form-factor and below which the FHM is dependent on the ABS design. This dependence on geometry (sliders length and/or ABS design) can been seen in Figs. 8 and 9. These figures show the form-factor FHM ratios or gains $\left((FHMgain)_{femto}/(FHMgain)_{pico}\right)$ for the same design plotted as a function of waviness wavelength. It can bee seen from Figs. 8 and 9 that in the waviness wavelength range of 7.5 mm to 20 mm the curve is constant. Below 7.5 mm the curves transition and increase to 100 % and beyond as the waviness wavelengths approach 0.3125 mm.

For ABS I and ABS II, the average values of the form-factor FHM ratios from waviness wavelength 7.5 mm to 20 mm are 52 % and 29 %, respectively. In this region, the FHM can be explained by Zhu's work showing that the FHM is proportional to the square of the slider length and the combined curvature of the slider and disk [5]:

$$FHM \propto L^2 Z'' \tag{2}$$

From this formulation, the form-factor FHM ratios should be:

$$\frac{FHM_{femto}}{FHM_{pico}} = \frac{L_f^2 \cdot Z_f''}{L_p^2 \cdot Z_p''} = \frac{\left(2/3\right)^2 \cdot L_p^2 \cdot \left(3/2\right) \cdot Z_p''}{L_p^2 \cdot Z_p''} = 66.7\% \tag{3}$$

where L_p and L_f are the lengths of the pico and femto sliders, respectively and Z_p'' and Z_f'' are the curvatures of the pico and femto sliders, respectively, calculated from the crown, *Z*, of the sliders:

$$Z(x) = 4R\left(\frac{x}{L} - \left(\frac{x}{L}\right)^2\right) \tag{4}$$

where *R* is the maximum value of crown shown in Table 1 and *x* is in the length direction of the slider. However, Zhu's formulation was for a simple taper-flat positive pressure slider and further simplified assuming a constant distributed pressure along the rails. The ABS designs evaluated in this study are much more complex, and it is found that for waviness wavelengths greater than 7.5 mm, the form-factor FHM ratios scale as $L^{2.6}$ and L^4 for ABS I and ABS II, respectively.

Below waviness wavelengths of 7.5 mm another mechanism causes geometric FHM. It has been recently seen that this geometric FHM is dependent on the ABS design and flying attitude (specifically the pressure profile), and the waviness wavelength [3]. This geometric FHM is primarily due to a phase shift between the slider's response at the transducer and the disk, ϕ, and secondarily due to an amplitude change, *B*. In this waviness wavelength range, 0.3125 mm to 7.5 mm, the slider's displacement can be written as:

$$s(x) = B\sin\left(\frac{2\pi}{\lambda}x + \phi\right) \tag{5}$$

In order to calculate the FHM gain, we subtract the disk's displacement in Eq. (1) from the slider's displacement in Eq. (5) and normalized by the disk's amplitude:

$$FHM_{geo} = \frac{B}{A}\sin\left(\frac{2\pi}{\lambda}x + \gamma\right) - \sin\left(\frac{2\pi}{\lambda}x\right) \tag{6}$$

This geometric FHM is the difference of two sinusoids with the same frequency but with different amplitude and a phase shift. This is illustrated in Fig. 10 which shows the disk

and slider displacements for ABS I in the pico form-factor for a disk waviness wavelength of 0.625 mm. The normalized amplitude, B/A, and the phase shift, f, are known to be dependent on a characteristic length, l, which is dependent on the ABS design and pressure profile rather than the slider's body length [3]. As the waviness wavelength decreases from 7.5 mm to 0.3125 mm, the form-factor FHM ratios for both ABS I and ABS II approach 100 %, showing that both form-factors exhibit similar levels of geometric FHM.

Clearly, for long waviness wavelengths, the ABS designs in the smaller form-factors out perform the larger form-factors. However, the FHM gain for long waviness wavelengths is extremely small, so the contribution to FHM is small. As the waviness wavelengths approach the length of the sliders, the amplitude ratios in Figs. 8 and 9 reach approximately 100%, showing FHM in this waviness wavelength range is independent of form-factor. By comparing ABS I to ABS II in Fig. 7, we see that the ABS II design exhibits approximately 50% less maximum FHM gain than the ABS I design for wavelengths in the vicinity of the slider body length for both form-factors. This result shows that ABS II is much less susceptible to geometric FHM than ABS I. Figures 8 and 9 are informative in comparing the ratio of $FHM_{p\text{-}p}$ / $DISK_{p\text{-}p}$ between form-factors of the same ABS designs, however it is useful to understand how this translates to FHM for an actual disk topography.

When the disk rotates, the disk's out-of-plane motion is composed of clamping distortions, disk flutter, and disk morphology, including waviness, micro-waviness and roughness in order of low to high frequency or long to short wavelength. For a typical "super-smooth" disk used in sub-10 nm FH applications, the out-of-plane displacement amplitudes decrease approximately exponentially as frequency increases or as wavelength decreases. Figures 11 and 12 show the FHM ratios for the ABS designs in the pico and femto form-factors and a measured typical "super-smooth" disk topography as a function of waviness wavelength. The disk displacement amplitudes were measured with a laser Doppler vibrometer and include wavelengths from 20 mm down to 0.3125 mm. To obtain the corresponding FHM, the disk amplitude was multiplied by the FHM ratio in Figs. 11 and 12. As shown in Figs. 11 and 12 the disk amplitudes follow approximately an exponentially increasing function of waviness wavelength and the

FHM ratio is approximately an exponentially decaying function of waviness wavelength. However, the FHM ratio curve decays faster than the disk function curve increases, so that when these two curves are combined to get FHM, the shorter waviness wavelengths influence the FHM more than the longer wavelengths.

In order to quantitatively compare the ABS designs and form-factors, we performed simulations using the measured disk topography. These simulation results are summarized in Table 3, which includes peak-to-peak and standard deviation (σ) of the FHM for ABS I and ABS II for the pico and femto form-factors. ABS I exhibited 22% less FHM for the femto than for the pico form-factor. Similarly, ABS II exhibited 32% less FHM for the femto than for the pico form-factor. Comparing only form-factors with the same ABS design, we see a significant decrease in FHM for the smaller form-factor. However, in cross-comparing ABS designs, ABS II is found to have 35%-40% less FHM than ABS I with the same form-factor. Additionally, ABS II in the pico form-factor exhibited 22% less FHM than ABS I in the femto form-factor.

DISCUSSION

By changing the form-factor of ABS designs and holding the design constant, we studied form-factor effects on dynamic and FHM performance. From the dynamic system properties, it is observed that, in general, the air bearing stiffnesses detrimentally decrease while the damping ratios beneficially increase as the form-factor is scaled from pico to femto. However, it is seen that these modal parameters determining the dynamic stability of the system do not scale proportionally with form-factor and are highly dependent on ABS design. The dynamic performance of ABS II is better than that of ABS I for two reasons. Firstly, it has the ability to maintain its stiffness by retaining a larger percentage of its bearing load capacity and by creating a higher peak pressure as the form-factor is scaled down from pico to femto. Secondly, the large number of transverse pressure contours on ABS II makes it highly damped compared to ABS I in both form-factors. Overall, a design's dynamic properties may not be enhanced by simply decreasing the form-factor. However with the proper design, both the modal stiffness and damping ratios can remain large leading to a dynamically more robust air bearing slider.

Another extremely important performance consideration is FHM. The largest contributor to FHM can be the geometric FHM, which is due to the disk morphology and other out-of-plane disk motions. The FHM ratios for the designs investigated were lower in amplitude for the smaller form-factor sliders for waviness wavelengths much longer than the slider body length. The femto form-factors exhibited 50% - 80% less FHM for long waviness wavelengths than the pico form-factor. However, as the disk waviness wavelength approach the slider body length, the FHM ratios becomes dependent on the ABS design and independent of form-factor. The ABS I design exhibited a gain in FHM ratio, approaching 100% and even slightly above 100%, for waviness wavelengths around the slider body length. However, for ABS II, a maximum FHM ratio of 50% was attained, half as much when compared to ABS I – regardless of form-factor.

To quantitatively compare form-factors and cross compare ABS designs, we conducted simulations using an actual measured disk topography. In comparing FHM for the same design, it was found that the smaller femto form-factor exhibited 22% - 32% less FHM than the larger pico form-factor. However, when cross comparing ABS designs, an even larger decrease in FHM was observed. The ABS II design demonstrated 35% - 40% less FHM compared to the ABS I design for both form-factors, pico and femto. Additionally, it was found that the pico form-factor of the ABS II design showed 22% less FHM compared to the femto form-factor of the ABS I design.

CONCUSION

By comparing the dynamic and FHM performance of pico and femto form-factor air bearing sliders designed for 100 Gbit/in^2 applications, it was found that the smaller form-factor exhibited an overall enhancement in performance when the ABS is properly designed. A beneficial increase in damping ratios and a detrimental decrease in modal stiffnesses was observed when scaling the form-factor from pico to femto. However, it was seen that if the ABS is designed to retain a larger percentage of its bearing load capacity and can maintain high peak pressure(s), the stiffness is not compromised dramatically by scaling down the form-factor. Also, a large number of transverse pressure gradients are extremely effective in increasing damping, and they further increase damping when the form-factor is scaled from pico to femto. FHM due to geometry is

composed of the superposition of two effects dependent on the overall length of the slider for long disk waviness wavelengths and dependent on the ABS design for shorter disk waviness wavelengths. For long waviness wavelengths, FHM was shown to be dependent on the sliders body length: proportional to $L^{2.6}$ and L^4 for ABS I and ABS II, respectively. For shorter waviness wavelengths, FHM was shown to be dependent on the ABS design and a phase shift between the slider's response at the transducer and the disk as well as an amplitude change in the slider's displacement. These two effects are demarked by a transition disk waviness wavelength of approximately 3 mm. By comparing femto to pico form-factors, it is seen that the femto exhibited lower FHM for waviness wavelengths greater than the sliders body length, however, it demonstrated similar levels of FHM for waviness wavelengths less than the sliders body length. By cross comparing ABS designs, it was found that significant improvements in FHM performance can also be attained by changing the ABS design and not decreasing the form factor. Simulations were performed using an actual measured disk topography which showed a decrease of 22 % to 32 % in FHM by scaling down the form-factor from pico to femto. However, by cross-comparing ABS designs, ABS II exhibited much less FHM even in comparing ABS II in the pico form-factor to ABS I in the femto form-factor. It is concluded that by simply scaling down the form-factor, enhanced performance is not always attained. However if special care is taken in the design of the ABS in order to maintain stiffness, increase damping and decrease geometric FHM, major improvements can be attained. Ultimately, to achieve the greatest performance, a smaller form-factor should be used with special care taken in the ABS design.

ACKNOWLEDGEMENTS

This work was supported by The Computer Mechanics Laboratory at the University of California, Berkeley, USA and the National Storage Industry Consortium (NSIC).

REFERENCES

[1] Mee, C. D., and Daniel, E. D., 1990, "*Magnetic Recording Handbook: Technology and Applications*," McGraw-Hill, Inc., New York, pp. 450-528.

[2] Wood, R., 2000 "The Feasibility of Magnetic Recording at 1 Terabit per Square Inch," *IEEE Transactions on Magnetics*, **36**, no. 1, pp. 36-42.

[3] Thornton, B. H., Nayak, A., and Bogy, D. B., "Flying Height Modulation Due to Disk Waviness of Sub-5 nm Flying Height Air Bearing Sliders," *ASME J. Tribology*, accepted for publication.

[4] Thornton, B. H., Bogy, D. B., and Bhatia, C. S., 2002, "The Effects of Disk Morphology on Flying Height Modulation: Experiment and Simulation," *IEEE Transactions on Magnetics*, Vol. 38, no. 1, pp.107-111.

[5] Zhu, L.-Y., Bogy, D. B., 1989, "Head-Disk Spacing Fluctuation due to Disk Topography in Magnetic Recording Hard Disk Files," *Tribology and Mechanics of Magnetic Storage Systems, STLE Special Publication*, SP-26, pp. 160-167.

[6] Zeng, Q. H., and Bogy, D. B., 1999, "Stiffness and Damping Evaluation of Air Bearing Sliders and New Designs with High Damping", *ASME J.Tribology*, Vol. 121, 341-347.

[7] Hu, Y., and Bogy, D. B., 1997, "Flying Characteristics of a Slider over Textured Surface Disks," *IEEE Transactions on Magnetics*, Vol. 33, no. 5, pp. 3196-3198.

[8] White, J. W., 1991, "The Transverse Pressure Contour Slider: Flying Characteristics and Comparisons with Taper-Flat and Cross-Cut Type Sliders," *Advances in Information Storage Systems*, Vol. 3, pp. 1-14.

[9] White, J. W., 1987, "Dynamic Response of the Transverse Pressure Contour Slider," *Tribology and Mechanics of Magnetic Storage Systems, STLE Special Publication*, SP-22, pp. 72-82.

[10] Tanaka, H., Yonemura, S, and Tokisue, H., 2001, "Slider Dynamics During Continuous Contact with Textured and Smooth Disks in Ultra Low Flying Height," *IEEE Transactions on Magnetics*, Vol. 37, no. 2, pp. 906-911.

	Air Bearing Design			
	ABS I		ABS II	
Form-Factor	Pico	Femto	Pico	Femto
Gram-Load [gm]	1.50	0.70	1.90	0.75
Positive Force [gm]	4.76	2.00	4.83	2.28
Negative Force [gm]	-3.26	-1.30	-2.93	-1.53
Pitch [μrad]	123.50	142.70	95.60	101.50
Roll [μrad]	-1.58	-1.43	-5.08	-2.97
Transducer FH [nm]	7.0	7.3	4.8	4.9
Crown [nm]	25.4	16.9	25.4	16.9
Camber [nm]	2.5	1.7	2.5	1.7
Base Recess [um]	2.5	1.7	2.5	1.7
Step Recess [um]	0.3	0.2	0.3	0.2

Table 1. Air bearing specifications and static flying attitude solution.

	Air Bearing Design			
	ABS I		ABS II	
Form-Factor	Pico	Femto	Pico	Femto
Normalized Peak Pressure (location A)	3.70	3.15	10.75	12.62
Normalized Peak Pressure (location B)	5.84	5.04	N/A	N/A

Table 2. Normalized peak pressures at locations A and B demarked in Fig 2 for ABS I and ABS II in the pico and femto form-factors.

	Air Bearing Design		
	ABS I	ABS II	ABS II / ABS I [%]
Femto Peak-to-Peak [nm]	1.52	0.90	**59%**
Femto σ [nm]	0.23	0.15	**63%**
Pico Peak-to-Peak [nm]	2.04	1.33	**65%**
Pico σ [nm]	0.30	0.18	**61%**
Femto/Pico (Peak-to Peak)	**74%**	**81%**	
Femto/Pico (σ)	**78%**	**68%**	

Table 3. FHM results from simulations with actual measured disk topography for ABS I and II in pico and femto form-factors.

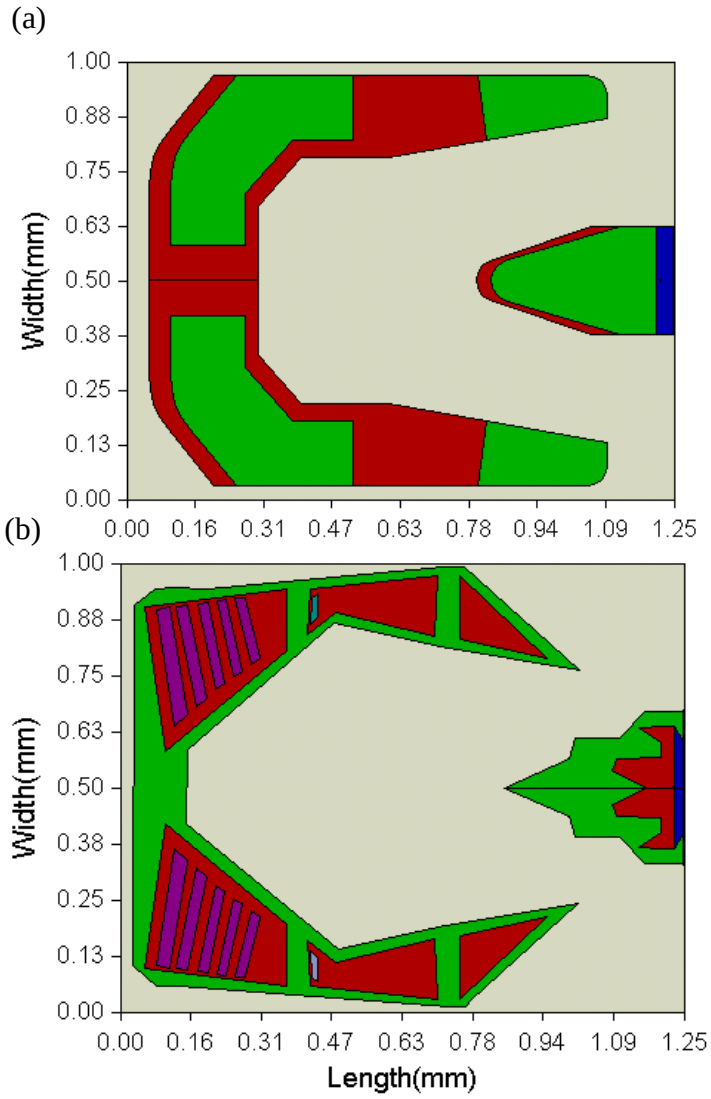

Fig. 1. Air bearing surface designs: (a) ABS I and (b) ABS II.

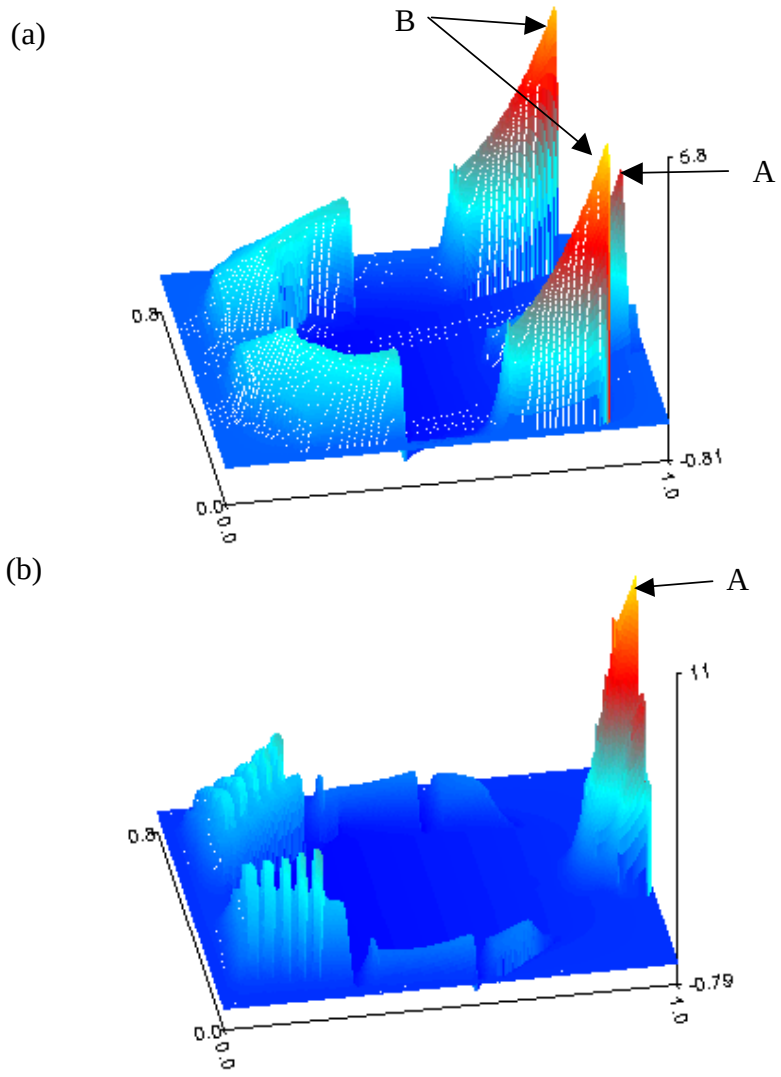

Fig. 2. Pressure profile generated by (a) ABS I, and (b) ABS II.

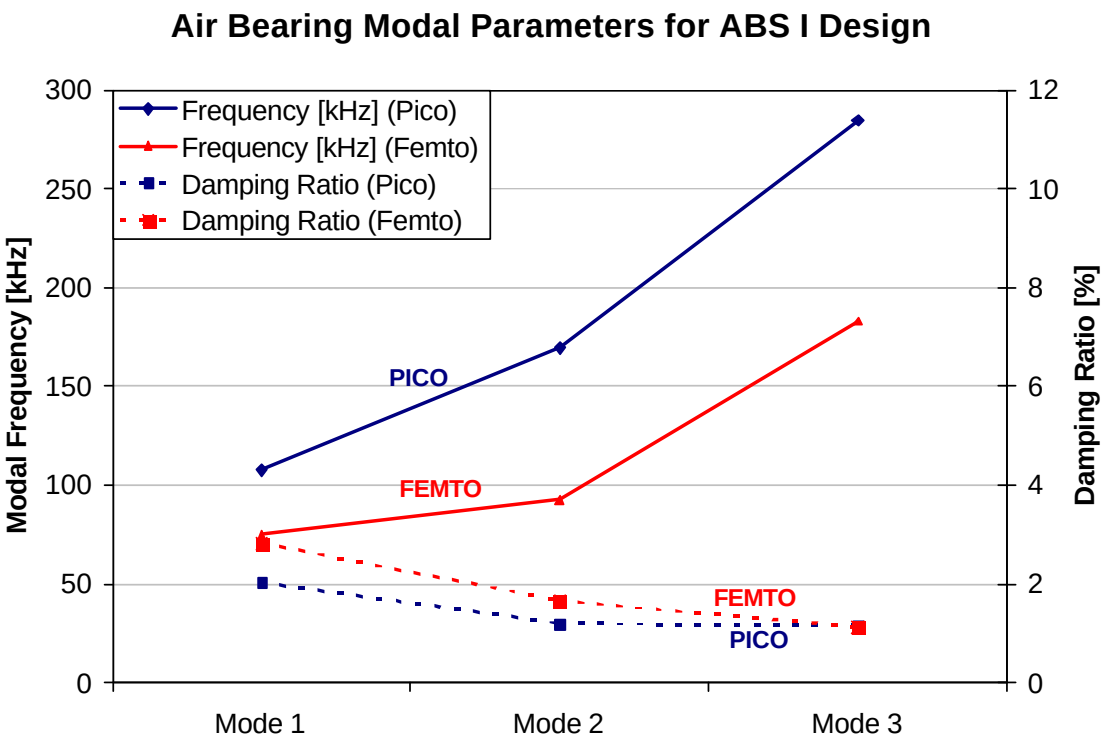

Fig. 3. Modal frequencies and damping ratios of the ABS I designs for the pico and femto form-factors.

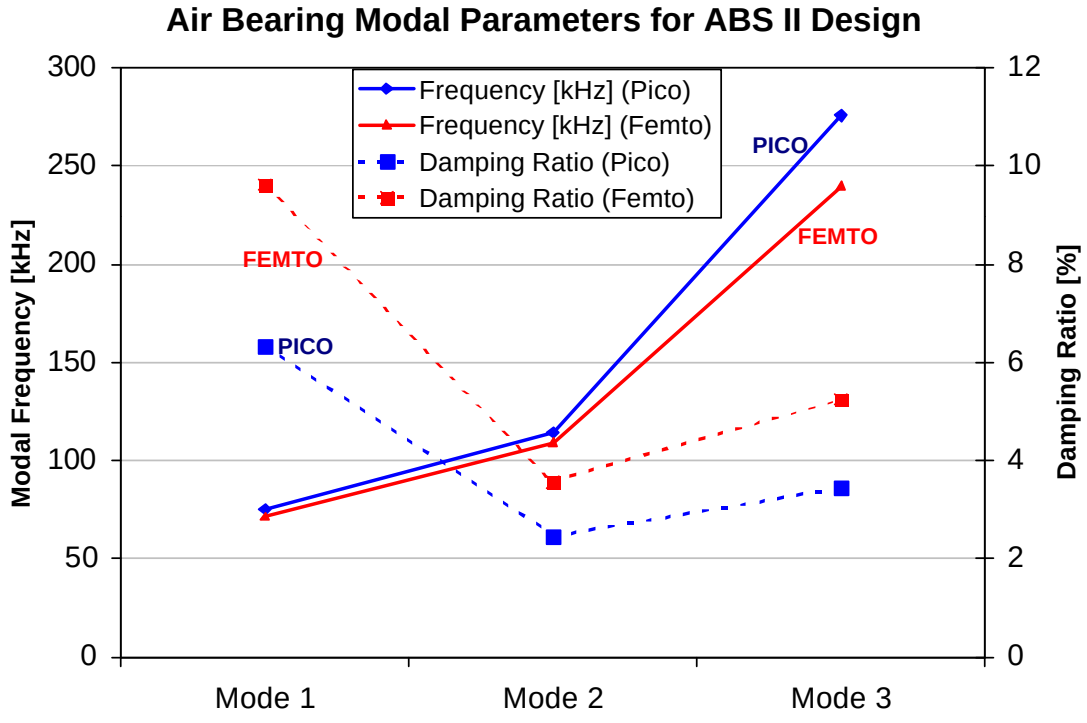

Fig. 4. Modal frequencies and damping ratios of the ABS II designs for the pico and femto form-factors.

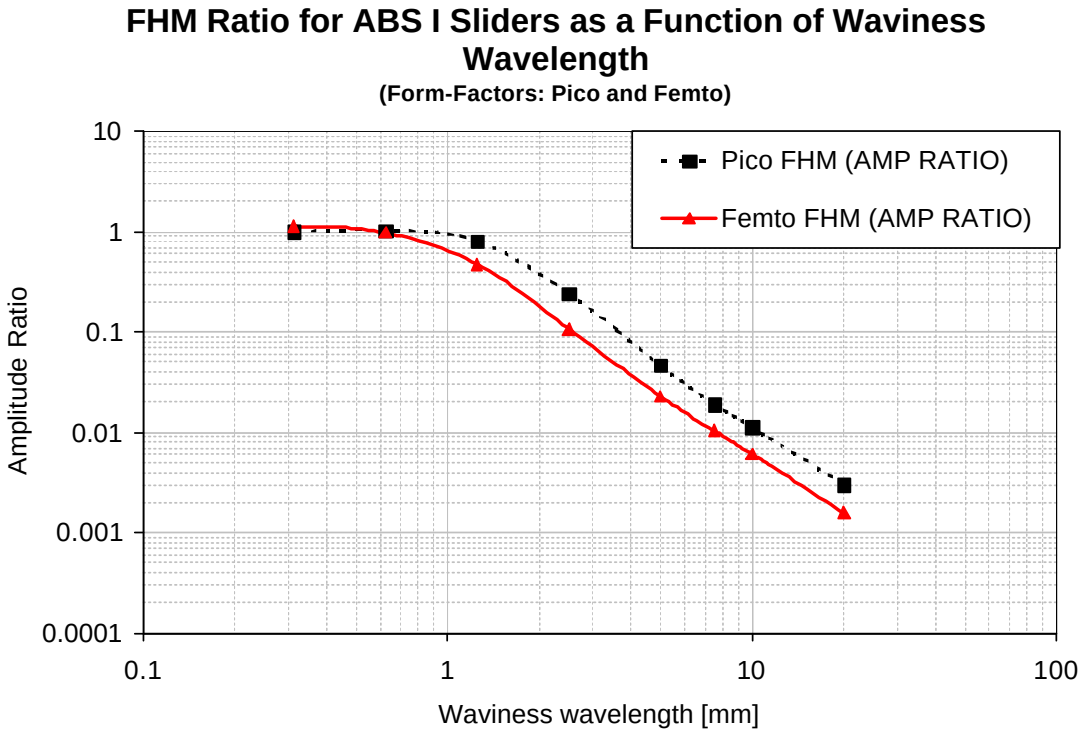

Fig. 5. FHM ratio or gain for the ABS I design ABS's as a function of disk waviness wavelength.

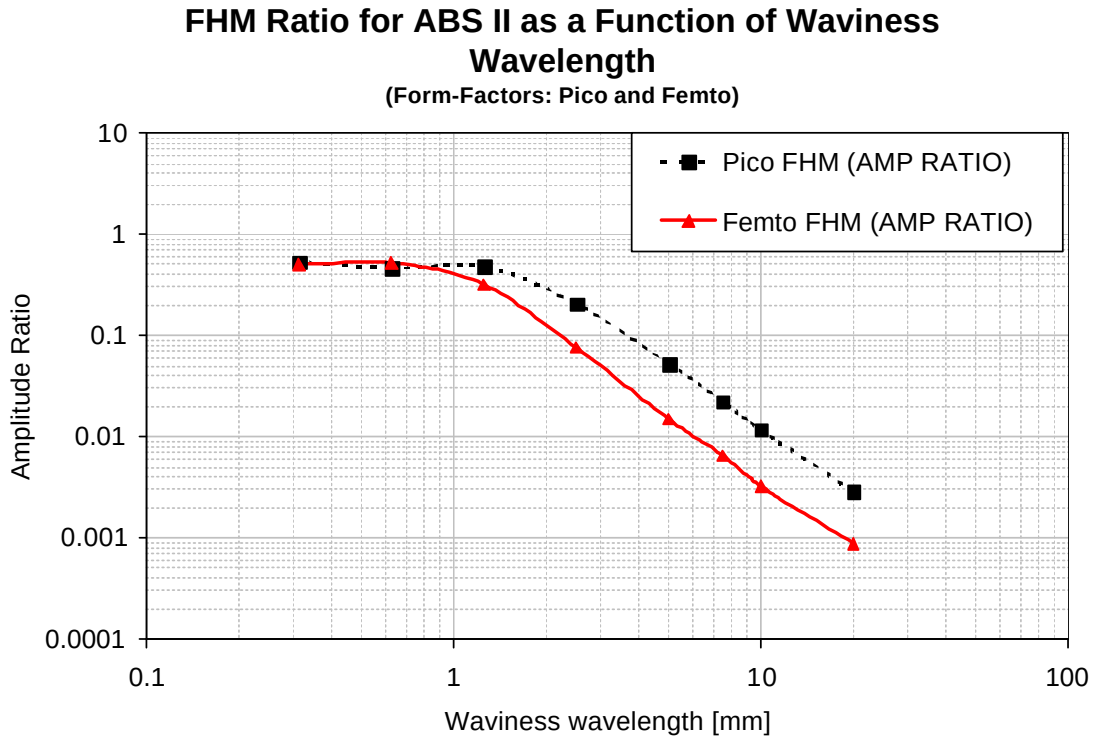

Fig. 6. FHM ratio or gain for the ABS II design ABS's as a function of disk waviness wavelength.

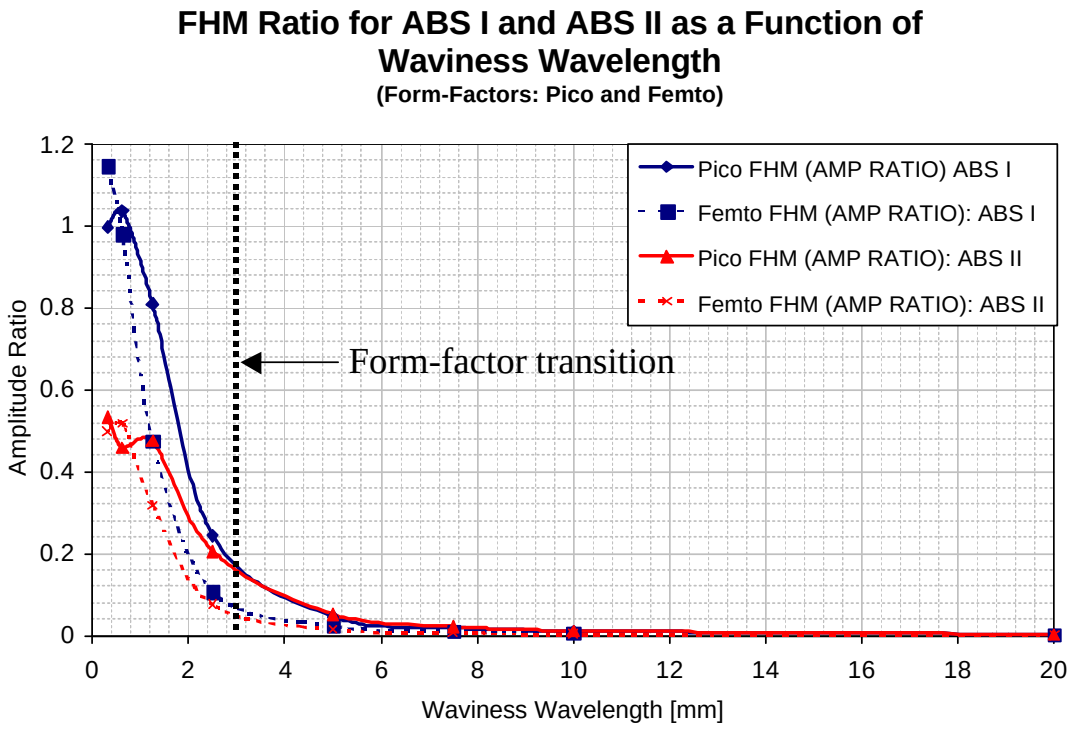

Fig. 7. FHM ratio or gain for the ABS I and ABS II ABS's as a function of disk waviness wavelength.

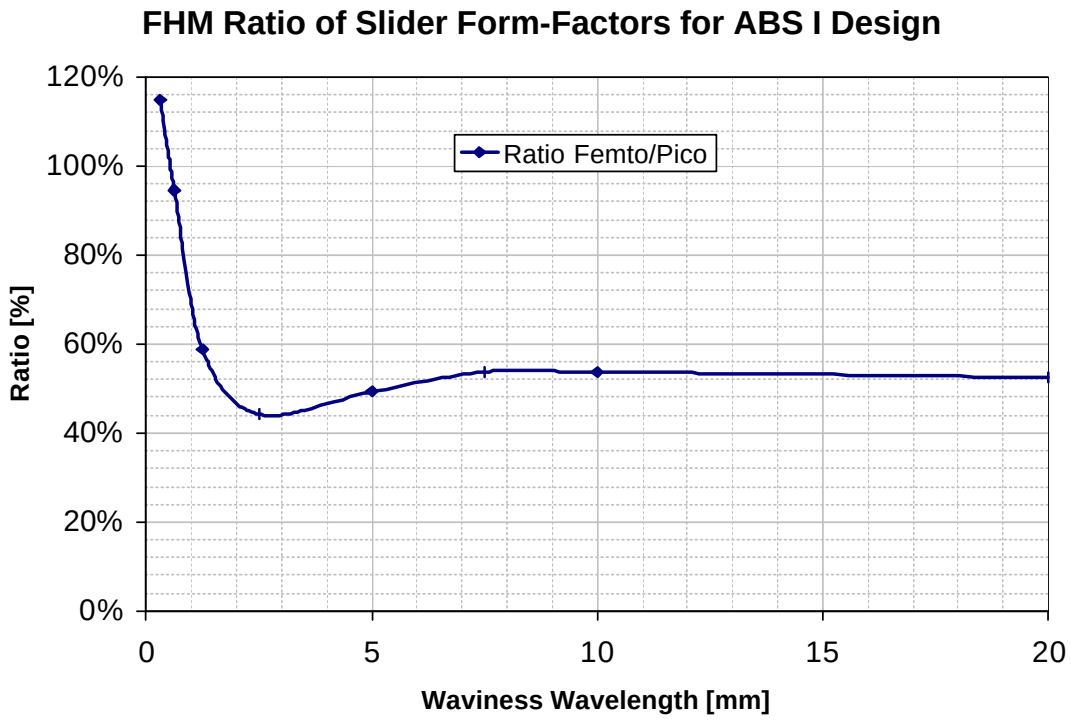

Fig. 8. The ratio of FHM ratios of the slider form-factors for the ABS I designs.

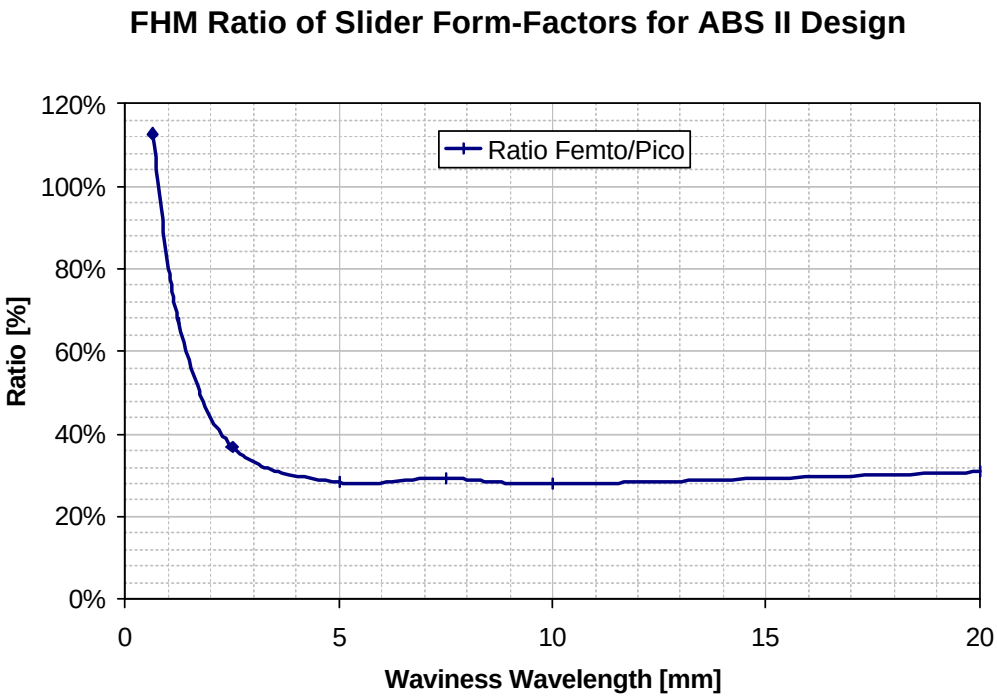

Fig. 9. The ratio of FHM ratios of the slider form-factors for the ABS II designs.

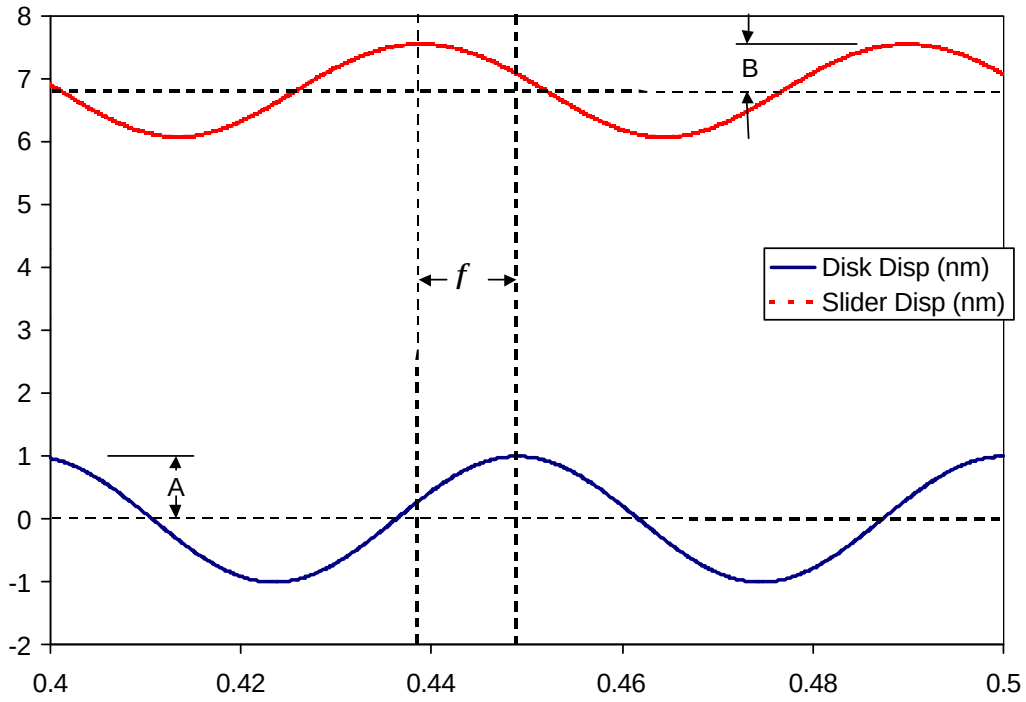

Fig. 10. Disk and slider displacement for ABS I in the pico form-factor for a disk waviness wavelength of 0.625 mm.

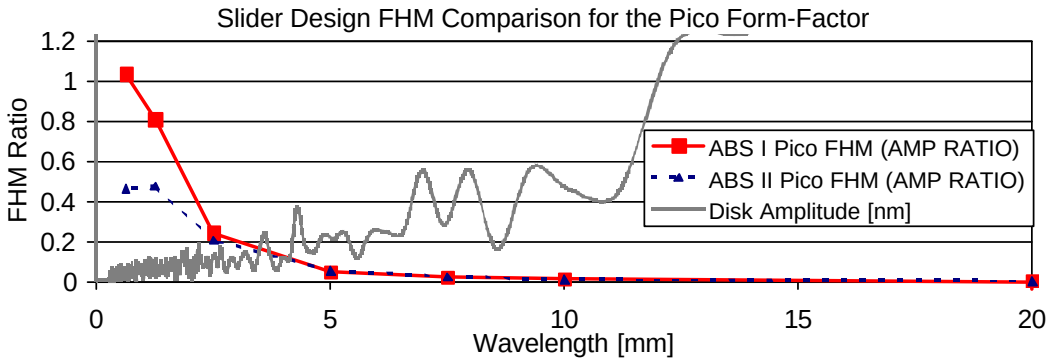

Fig. 11. Slider design comparison of the FHM ratios for the pico form-factor with a measured disk topography overlaid.

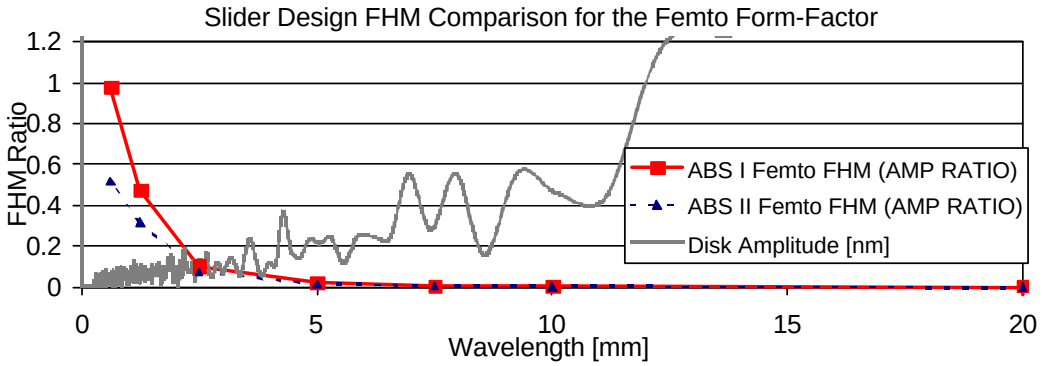

Fig. 12. Slider design comparison of the FHM ratios for the femto form-factor with a measured disk topography overlaid.